INTERNATIONAL JOURNAL FOR NUMERICAL METHODS IN FLUIDS
Int. J. Numer. Meth. Fluids **29**: 207–227 (1999)

A TIME-ACCURATE SCHEME FOR THE CALCULATIONS OF UNSTEADY REACTIVE FLOWS AT LOW MACH NUMBER

C. CORVELLEC[a], P. BRUEL[a,*,1] AND V.A. SABEL'NIKOV[b]

[a] *Laboratoire de Combustion et de Détonique, UPR No. 9028 du CNRS, ENSMA, B.P. 109, 86960 Futuroscope Cedex, France*
[b] *Central Aero-Hydrodynamic Institute (TsAGI), Zhukovsky, Moscow Region, 140160, Russian Federation*

SUMMARY

The artificial compressibility method is extended to the case of unsteady turbulent reacting flows at low Mach number. The resulting scheme is applied to the calculation of a propagating one-dimensional (1D) planar turbulent flame with a realistic heat release parameter. An eddy break-up-like approach, with a conventional gradient expression for the turbulent fluxes, is retained to model this reacting turbulent flow. A quenched form of the mean reaction rate is used to ensure the existence of a steady regime of propagation, for which the present results are compared with those obtained by a steady analysis of the mean flame brush structure, with excellent agreement. A sensitivity analysis of the convergence rate to the values of the artificial compressibility factor and the pseudo-time is carried out. It is shown that a reduced artificial compressibility factor of 5–10, combined with a pseudo-Courant number of ≈ 1000, represents a good compromise to optimize the convergence rate. Copyright © 1999 John Wiley & Sons, Ltd.

KEY WORDS: artificial compressibility; premixed turbulent combustion; low Mach number; unsteady flow

1. INTRODUCTION

Unsteady reacting flows for which the density changes are mostly related to the heat release due to combustion are often encountered in systems of practical interest, such as furnaces or turbojet engines. For such flows characterized by a low Mach number (i.e. $Ma \ll 1$), the pressure, supposed to be *thermodynamically* constant, is influencing the flow motion only through its spatial derivatives present in the momentum equations [1]. Thus, the fact that the pressure field cannot be extracted from the equation of state implies that a specific procedure has to be derived to accurately compute this pressure field. Specific techniques, such as the PISO [2] or the SIMPLE(R) [3] procedures, can be used to deal with these kind of flows, but they present the drawback of leading to program structures very different from those of programs developed to cope with inert compressible flows. A direct consequence of this is a greater investment in time by the end-user who has to get acquainted with several different programs at the expense of a loss of immediate efficiency. A way of preserving a community

* Correspondence to: Laboratoire de Combustion et de Détonique, UPR No. 9028, CNRS, ENSMA, B.P. 109, 86960 Futuroscope Cedex, France.
[1] Tel.: +33 549498164; fax: +33 549498176; e-mail: bruel@lcd.ensma.fr

CCC 0271–2091/99/020207–21$17.50

Received January 1998
Revised March 1998

of structure as large as possible between programs able to cope with compressible flows or low Mach number flows, is to have recourse in the latter case to the artificial compressibility (AC) method originally proposed by Chorin [4]. The AC method is a well-established numerical approach for solving the incompressible Navier–Stokes equations. Its success is largely due to a clear physical interpretation of the procedure: the addition of a non-stationary pressure term in the continuity equation introduces waves of finite speed that distribute the static pressure throughout the computational domain. The results are physically meaningful when a converged solution in pseudo-time is obtained. An attractive characteristic of the AC method is that programs originally developed to deal with compressible inert flows require only minor modifications to incorporate this approach, thus saving a lot of computational effort and enlarging the variety of flows that these programs can cope with. The AC method has been recently extended to the calculation of steady isenthalpic reacting flows in the limit of a low Mach number [5]. The resulting scheme has been successfully applied to deal with the complex flow geometry of a turbulent flame stabilized in a stagnation point flow [6]. In all the aforementioned cases of steady inert and isenthalpic reacting flow calculations, the artificial compressibility is introduced in the continuity equation by writing:

$$\frac{\partial p}{\partial \tau} + \beta \ \mathrm{div}(\rho \boldsymbol{u}) = 0, \tag{1}$$

where p is the pressure, τ is the pseudo-time, ρ is the density, $\boldsymbol{u}$ is the flow velocity vector and β is the artificial compressibility factor whose value strongly influences the convergence rate and has to be chosen carefully. The density is known from the equation of state given by, with the usual notations, (i) $\rho = cst$ for inert incompressible flows and (ii) $\rho T = cst$ for isenthalpic reactive flows in the limit of a low Mach number. As far as unsteady flows are concerned, only inert flows have been dealt with using the AC method by, among others, Peyret [7], Choi and Merkle [8], Soh and Goodrich [9], Granier *et al.* [10] and Rogers and Kwak [11]. In these studies, the physical time t is introduced in the momentum equation, while the continuity equation (Equation (1)) remains unchanged. For each physical time step, Δt, the convergence of the iteration AC cycle in pseudo-time τ leads to the desired time varying solution. The artificial compressibility method appears to be sufficiently versatile to justify a still on-going process of improvement of either its efficiency [12.13] or its domain of applicability [5,10]. The aim of this paper is to propose and describe the extension of the AC method to unsteady reacting flows in the limit of a low Mach number. Section 2 presents the time-accurate scheme based on the artificial compressibility method. A description of the flow geometry used to test the present scheme is given in Section 3. The set of equations to be solved, together with the details of the spatial discretization, mesh adaptation and boundary conditions are presented in Section 4. The results are presented in Section 5. They put into evidence the capability of the proposed time-accurate scheme to deal with the unsteadiness of a reacting flow. The results of a sensitivity analysis of the convergence rate to the value of the artificial compressibility factor and the pseudo-time step are also given and will help people interested in using the scheme to begin with a reasonable choice for these parameters.

2. ARTIFICIAL COMPRESSIBILITY SCHEME

The generic vector form of the system that describes the evolution of the relevant variables (the density, the velocity component(s), the energy or the temperature) in a laminar or turbulent reactive flow can be formally written as (presented here in one dimension for simplicity):

$$\frac{\partial \boldsymbol{q}}{\partial t}+\frac{\partial(\boldsymbol{F}^{\mathrm{i}}-\boldsymbol{F}^{v})}{\partial x}=\boldsymbol{S}, \tag{2}$$

where $\boldsymbol{F}^{\mathrm{i}}$ represents the inviscid terms, $\boldsymbol{F}^{v}$ groups all the other fluxes (either laminar or turbulent or both) and $\boldsymbol{S}$ stands for all the source terms associated in particular with the combustion process, and possibly the turbulence modeling. The dimension of the vector of unknowns $\boldsymbol{q}$ depends on the combustion and, if relevant, on the turbulence modeling.

The present time-accurate scheme is the result of the combination of the approaches followed by Bruel *et al.* [5] for steady reacting flows and by Soh and Goodrich [9] and Rogers and Kwak [11] for unsteady inert flows. System (2) is modified by introducing a *pseudo-time*, τ, leading to the following form:

$$\frac{\partial \hat{\boldsymbol{q}}}{\partial t}+\frac{\partial \boldsymbol{q}^{\mathrm{ac}}}{\partial \tau}+\frac{\partial(\boldsymbol{F}^{\mathrm{ac}}-\boldsymbol{F}^{v})}{\partial x}=\boldsymbol{S}, \tag{3}$$

with

$$\boldsymbol{q}^{\mathrm{ac}}=\mathbf{I}_1\cdot\boldsymbol{q}, \qquad \boldsymbol{F}^{\mathrm{ac}}=\mathbf{I}_2\cdot\boldsymbol{F}^{\mathrm{i}}, \qquad \hat{\boldsymbol{q}}=\mathbf{I}_2\cdot\boldsymbol{q}, \tag{4}$$

where the matrices $\mathbf{I}_1$ and $\mathbf{I}_2$ are defined by

$$\mathbf{I}_1=\begin{bmatrix} p/\rho & 0 & \cdots & 0\\ 0 & 1 & \ddots & \vdots\\ \vdots & \ddots & \ddots & 0\\ 0 & \cdots & 0 & 1\end{bmatrix}, \qquad \mathbf{I}_2=\begin{bmatrix} \beta & 0 & \cdots & 0\\ 0 & 1 & \ddots & \vdots\\ \vdots & \ddots & \ddots & 0\\ 0 & \cdots & 0 & 1\end{bmatrix}. \tag{5}$$

The physical unsteady terms are treated as source terms during the course of the iteration cycle in pseudo-time. Thus, starting from the known solution at time t_n and for a physical time step Δt, the desired solution at time $t_{n+1}=t_n+\Delta t$ is obtained when a *steady state* in pseudo-time τ is reached, i.e. when $\partial \boldsymbol{q}^{\mathrm{ac}}/\partial\tau$ tends to zero. Consequently, for each physical time step, the following system has to be solved:

$$\left.\frac{\partial \boldsymbol{q}^{\mathrm{ac}}}{\partial \tau}\right|^{n+1,v+1}+\left.\frac{\partial(\boldsymbol{F}^{\mathrm{ac}}-\boldsymbol{F}^{v})}{\partial x}\right|^{n+1,v+1}=\boldsymbol{S}|^{n+1,v+1}-\left.\frac{\partial \hat{\boldsymbol{q}}}{\partial t}\right|^{n+1,v+1}, \tag{6}$$

where superscript v refers to the iteration cycle in pseudo-time.

Many different options can be considered to treat the different terms in system (6). Here, rather simple standard techniques are retained to deal with these terms, although alternative and possibly more refined options could be considered in the future if specific requirements in terms of either precision or rate of convergence are to be met.

Beginning with the right-hand-side of (6), a three-point backward implicit formula of second-order accuracy is chosen to express the physical time derivative, namely:

$$\left.\frac{\partial \hat{\boldsymbol{q}}}{\partial t}\right|^{n+1,v+1}=3\,\frac{\hat{\boldsymbol{q}}|^{n+1,v+1}-\hat{\boldsymbol{q}}|^{n}}{2\Delta t}-\frac{\hat{\boldsymbol{q}}|^{n}-\hat{\boldsymbol{q}}|^{n-1}}{2\Delta t}+O(\Delta t^2). \tag{7}$$

The stability of the scheme can be enhanced in a simple way by treating implicitly in the delta form, the term $\hat{\boldsymbol{q}}|^{n+1,v+1}-\hat{\boldsymbol{q}}|^{n}$. Indeed, using a linearization around the previous estimate of the solution, i.e. $\hat{\boldsymbol{q}}^{\mathrm{ac}}|^{n+1,v}$, one obtains:

$$\left.\frac{\partial \hat{\boldsymbol{q}}}{\partial t}\right|^{n+1,v+1}=\frac{3}{2\Delta t}\left[\left.\frac{\partial \hat{\boldsymbol{q}}}{\partial \boldsymbol{q}^{\mathrm{ac}}}\right|^{n+1,v}\cdot[\Delta \boldsymbol{q}^{\mathrm{ac}}]^{n+1,v}\right]+3\,\frac{\hat{\boldsymbol{q}}|^{n+1,v}-\hat{\boldsymbol{q}}|^{n}}{2\Delta t}-\frac{\hat{\boldsymbol{q}}|^{n}-\hat{\boldsymbol{q}}|^{n-1}}{2\Delta t}+O(\Delta t^2), \tag{8}$$

where $[\Delta \boldsymbol{q}^{\mathrm{ac}}]^{n+1,v}$ stands for $(\boldsymbol{q}^{\mathrm{ac}}|^{n+1,v+1} - \boldsymbol{q}^{\mathrm{ac}}|^{n+1,v})$ and '$\cdot$' indicates a matrix product. The source term $\boldsymbol{S}$ is classically decomposed in a negative part, treated implicitly, namely

$$\boldsymbol{S}_- \Big|^{n+1,v+1} = \boldsymbol{S}_- \Big|^{n+1,v} + \frac{\partial \boldsymbol{S}_-}{\partial \boldsymbol{q}^{\mathrm{ac}}}\Bigg|^{n+1,v} \cdot [\Delta \boldsymbol{q}^{\mathrm{ac}}]^{n+1,v} + O(\Delta\tau^2), \tag{9}$$

and in a positive part, treated explicitly, as

$$\boldsymbol{S}_+ \Big|^{n+1,v+1} = \boldsymbol{S}_+ \Big|^{n+1,v} + O(\Delta\tau). \tag{10}$$

Consider now the left-hand-side of (6). Since the discretization of $(\partial \boldsymbol{q}^{\mathrm{ac}}/\partial\tau)$ is influencing only the convergence path of the iteration cycle in pseudo-time, a simple implicit Euler formulation of first-order is retained for this term:

$$\frac{\partial \boldsymbol{q}^{\mathrm{ac}}}{\partial\tau}\Bigg|^{n+1,v+1} = \frac{\boldsymbol{q}^{\mathrm{ac}}|^{n+1,v+1} - \boldsymbol{q}^{\mathrm{ac}}|^{n+1,v}}{\Delta\tau} + O(\Delta\tau). \tag{11}$$

As far as the vectors $\boldsymbol{F}^{\mathrm{ac}}$ and $\boldsymbol{F}^v$ are concerned, and due to the fact that a one-dimensional flow is considered, an implicit treatment of these terms in pseudo-time is easy to implement as follows:

$$\frac{\partial(\boldsymbol{F}^{\mathrm{ac}} - \boldsymbol{F}^v)}{\partial x}\Bigg|^{n+1,v+1} = \frac{\partial}{\partial x}\left[\frac{\partial(\boldsymbol{F}^{\mathrm{ac}} - \boldsymbol{F}^v)}{\partial \boldsymbol{q}^{\mathrm{ac}}}\Bigg|^{n+1,v} \cdot [\Delta \boldsymbol{q}^{\mathrm{ac}}]^{n+1,v}\right] + \frac{\partial(\boldsymbol{F}^{\mathrm{ac}} - \boldsymbol{F}^v)}{\partial x}\Bigg|^{n+1,v} + O(\Delta\tau^2). \tag{12}$$

It should be pointed out that in the case of multidimensional flows, some explicit treatment may be the only practical way to deal with some of the components of $\boldsymbol{F}^v$, especially those involving cross-derivatives.

Finally, with relations (8)–(12), system (6) can be written in the following form:

$$\left[\left(\frac{1}{\Delta\tau}\,\mathbf{I}. + \frac{\partial}{\partial x}\,\mathbf{A}. - \frac{\partial}{\partial x}\,\mathbf{P}. - \mathbf{C}. + \frac{3}{2\Delta t}\,\mathbf{G}.\right)^{n+1,v} [\Delta \boldsymbol{q}^{\mathrm{ac}}]^{n+1,v}\right]$$
$$= -\frac{\partial(\boldsymbol{F}^{\mathrm{ac}} - \boldsymbol{F}^v)^{n+1,v}}{\partial x} + \boldsymbol{S}\Big|^{n+1,v} - 3\,\frac{\hat{\boldsymbol{q}}\Big|^{n+1,v} - \boldsymbol{q}\Big|^n}{2\Delta t} + \frac{\hat{\boldsymbol{q}}\Big|^n - \hat{\boldsymbol{q}}\Big|^{n-1}}{2\Delta t}, \tag{13}$$

where $\mathbf{I}$ is the identity matrix, and the various Jacobian matrices are defined by:

$$\mathbf{A}^{(n+1,v)} = \frac{\partial \boldsymbol{F}^{\mathrm{ac}}}{\partial \boldsymbol{q}^{\mathrm{ac}}}\Bigg|^{n+1,v}, \qquad \mathbf{P}^{(n+1,v)} = \frac{\partial \boldsymbol{F}^v}{\partial \boldsymbol{q}^{\mathrm{ac}}}\Bigg|^{n+1,v}, \tag{14}$$

$$\mathbf{C}^{(n+1,v)} = \frac{\partial \boldsymbol{S}_-}{\partial \boldsymbol{q}^{\mathrm{ac}}}\Bigg|^{n+1,v}, \qquad \mathbf{G}^{(n+1,v)} = \frac{\partial \hat{\boldsymbol{q}}}{\partial \boldsymbol{S}^{\mathrm{ac}}}\Bigg|^{n+1,v}. \tag{15}$$

System (13) is very similar in its formal aspect to a fractional step of implicit-factored schemes, such as Beam and Warming-like schemes [23] for solving unsteady inert compressible flows. Thus, if one has a program that uses such a scheme, the implementation of the AC approach to cope with low Mach number flows (reacting or inert) is rather straightforward and the resulting program has a structure that strongly resembles that of the original code.

3. DESCRIPTION OF THE TEST CASE

The above expressions represent the basis of the present time-accurate scheme. In order to detail the various vectors and matrices involved in the scheme, it has now to be applied to a

given flow geometry. Here, the geometry of an idealized 1D turbulent premixed flame that propagates in a turbulent medium is retained. The choice of this geometry, schematically represented in Figure 1, is dictated by its simplicity, which allows an unambiguous evaluation of the numerical scheme as soon as the modeling of the flow is clearly given. Such a modeling is chosen here to ensure that there exists a unique steady regime of propagation of the mean flame brush. This choice is encouraged due to the fact that when such a regime is reached, a direct comparison with solutions obtained from a numerical analysis of the steady equations (written in a co-ordinate system attached to the mean flame brush) can be performed. In addition, it is much easier to reveal the sensitivity of the convergence rate to the various parameters that are characterizing this time-accurate scheme when the time scale associated with the flame propagation remains constant after a given period of time.

3.1. Modeling of the reacting flow

Since the present study is concerned with the method of solution rather than the modeling of the combustion process itself, little will be said about the combustion model. The hypothesis of the eddy break-up model [14], which can be considered as being representative of mixing controlled reaction rate models and which is extensively used in calculations of practical systems such as combustion chambers of turbojet engines or industrial furnaces, is adopted. The combustion process is represented, for the instantaneous field, through the evolution of a single bi-valued progress variable $c = (T - T_r)/(T_b - T_r)$, where subscripts r and b correspond to the reactants ($c = 0$) and the fully burnt products ($c = 1$) respectively. The heat release parameter χ, which characterizes the gas expansion associated with the heat release, is given by $\chi = (T_b - T_r)/T_r$. In the limit of a low Mach number, the static pressure is thermodynamically constant, i.e. the density variations are uniquely related to the temperature changes due to the heat release, but the pressure gradient is kept in the momentum equation. Thus, the equation of state reads $\rho T = \rho_r T_r = \rho_b T_b$. The flame under consideration propagates through high Reynolds number turbulence, which is supposed to be homogeneous and isotropic upstream of the flame. For simplicity, the turbulence field is chosen to be steady and the turbulence kinetic energy, k, and its dissipation rate, ε, are constant everywhere in the flow and equal to the values k_r and ε_r chosen to prevail in the reactants. The values of k_r and ε_r are determined via the prescription of the rms velocity $u'_r = \sqrt{u_r^2}$ and the integral length scale l_i with the following classical relations:

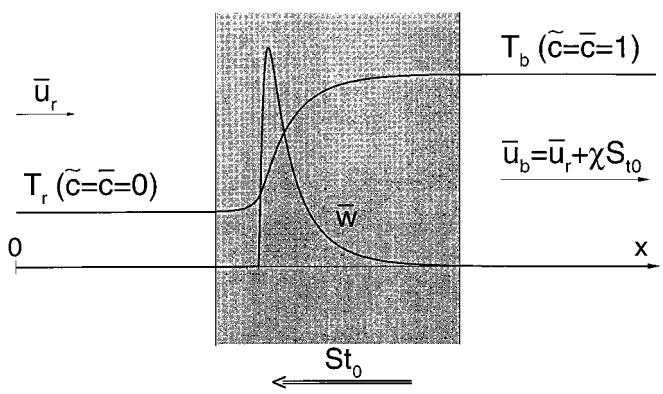

Figure 1. Schematic of the 1D planar turbulent flame.

$$k_r = \frac{3}{2} u_r^2, \qquad \varepsilon_r = C_\mu^{0.75} k_r^{3/2} / l_t,$$

with $C_\mu = 0.09$.

A conventional gradient assumption is retained to express the turbulent fluxes of mass and momentum. According to this flow description, and neglecting the laminar contribution to the effective viscosity (high Reynolds number flow), the propagation of the turbulent flame brush is described by system (2) with:

$$\boldsymbol{q} = \begin{bmatrix} \bar{\rho} \\ \bar{\rho}\tilde{u} \\ \bar{\rho}\tilde{c} \end{bmatrix}, \tag{16}$$

$$\boldsymbol{F}^i = \begin{bmatrix} \bar{\rho}\tilde{u} \\ \bar{\rho}\tilde{u}^2 + \bar{p} + \frac{2}{3}\bar{\rho}k_r \\ \bar{\rho}\tilde{u}\tilde{c} \end{bmatrix}, \qquad \boldsymbol{F}^v = \begin{bmatrix} 0 \\ \frac{4}{3}\mu_t \dfrac{\partial \tilde{u}}{\partial x} \\ \dfrac{\mu_t}{Sc_t} \dfrac{\partial \tilde{c}}{\partial x} \end{bmatrix}, \qquad \boldsymbol{S} = \begin{bmatrix} 0 \\ 0 \\ \bar{w} \end{bmatrix}, \tag{17}$$

where, for a given quantity Φ, $\tilde{\Phi} = \overline{\rho\Phi}/\bar{\rho}$ stands for the classical Favre mass-weighted average. The turbulent eddy viscosity coefficient is given by

$$\mu_t = C_\mu \bar{\rho} \frac{k_r^2}{\varepsilon_r} \tag{18}$$

and Sc_t is a turbulent Schmidt number. System (2) is supplemented by the equation of state $\overline{\rho T} = cst$ written in terms of ρ and c as:

$$\bar{\rho} = \frac{\rho_r}{1 + \chi\tilde{c}}. \tag{19}$$

3.2. Mean reaction rate

As far as the propagation properties of the flame brush are concerned, it is well-known that the form of the mean reaction rate plays a central role. A comprehensive survey of this question can be found in [15]. In order to test the present numerical scheme, a quenched form of the mean reaction rate is chosen. Indeed, quenching the mean reaction rate by setting it to zero as soon as the progress variable is below some quenching value, c^*, ensures the obtaining of a unique steady regime of propagation [16,17]. The resulting propagation velocity is in a one-to-one correspondence with the value of c^* [18]. The quenched mean reaction rate can be either a non-continuous [17,18] or a continuous [19] function of the mean progress variable $\tilde{c}$. A non-continuous form of $\bar{w}$ presents the drawback of introducing a discontinuity of the pressure gradient within the mean flame brush at the point where the progress variable reaches the quenching value c^*. Such a discontinuity makes testing of any numerical scheme difficult because the results are always sensitive to the mesh refinement in the vicinity of the pressure gradient discontinuity. Consequently, in

the present study, a continuous quenched form of the mean reaction rate $\bar{w}$ is used, which is given by:

$$\bar{w} = \begin{cases} 0 & \text{if } \tilde{c} \le \chi c^* \\ C_w(1+\chi)\dfrac{(\tilde{c}-\chi c^*)(1-\tilde{c})}{(1+\chi\tilde{c})^2} & \text{otherwise} \end{cases}. \tag{20}$$

Only a brief description of the procedure used to determine the value of c^* that corresponds to the desired value of the propagation velocity S_{t_0}, is given here. Following the procedure originally developed by Kolmogorov *et al.* [24] (thereafter referred to as KPP), the *steady* $\tilde{c}$ equation, written in a co-ordinate system attached to the mean flame brush, is transformed into a first-order differential equation for $P = (\mu_t/mSc_t)(\mathrm{d}\tilde{c}/\mathrm{d}x)$, where the mass flow m through the flame brush, i.e. $m = \rho_r S_{t_0}$, is an eigenvalue as soon as $\bar{w}$ is quenched. Using the numerical technique developed by Sabel'nikov *et al.* [18], this P equation is solved in the phase space by a highly accurate shooting technique procedure based on a fourth-order Runge–Kutta procedure. A Newton–Raphson cycle allows the determination of the c^* value that corresponds to the desired value of the propagation velocity. The knowledge of P permits the calculations of the $\tilde{c}$ profile, as well as the velocity and the pressure gradient profiles. Thus, when, with the present AC-based time-accurate scheme, the *steady* regime of propagation is reached, the accuracy of the calculated profiles as well as the value of their propagation velocity can be compared with those provided by the aforementioned highly accurate Runge–Kutta procedure. With the above form of $\bar{w}$, the two contributions $\boldsymbol{S}_+$ and $\boldsymbol{S}_-$ to the source term $\boldsymbol{S}$ are given by:

$$\boldsymbol{S}_+ = \begin{bmatrix} 0 \\ 0 \\ C_w\dfrac{(1+\chi)}{(1+\chi\tilde{c})}(\tilde{c}-\chi c^*(1-\tilde{c})) \end{bmatrix}, \qquad \boldsymbol{S}_- = \begin{bmatrix} 0 \\ 0 \\ -C_w\dfrac{(1+\chi)}{(1+\chi\tilde{c})^2}\tilde{c}^2 \end{bmatrix}. \tag{21}$$

4. FINAL SYSTEM OF EQUATIONS

By retaining the modeling presented in the previous section, the various vectors and matrices defined in Section 2 and appearing in system (13) are given by:

$$\boldsymbol{q}^{\mathrm{ac}} = \begin{bmatrix} \bar{p} \\ \bar{\rho}\tilde{u} \\ \bar{\rho}\tilde{c} \end{bmatrix}, \qquad \hat{\boldsymbol{q}} = \begin{bmatrix} \beta\bar{\rho} \\ \bar{\rho}\tilde{u} \\ \bar{\rho}\tilde{c} \end{bmatrix}, \qquad \boldsymbol{F}^{\mathrm{ac}} = \begin{bmatrix} \beta\bar{\rho}\tilde{u} \\ \bar{\rho}\tilde{u}^2 + \bar{p} + \frac{2}{3}\bar{\rho}k_r \\ \bar{\rho}\tilde{u}\tilde{c} \end{bmatrix}, \tag{22}$$

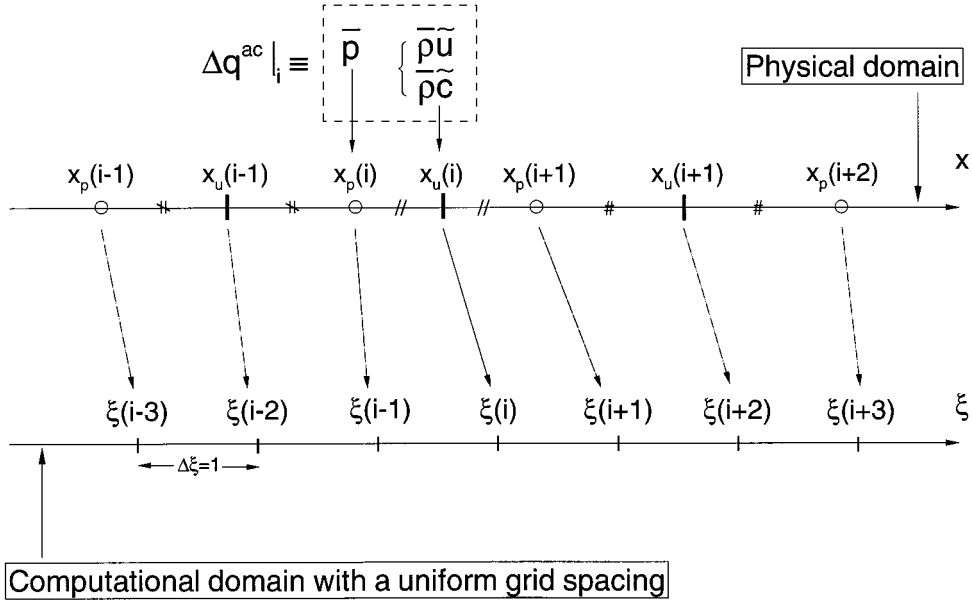

Figure 2. Stencil retained for the physical and the computational meshes.

$$\mathbf{A}^{(n+1,v)} = \begin{bmatrix} 0 & \beta & 0 \\ 1 & 2\tilde{u} & \chi\tilde{u}^2 - \frac{2}{3}\chi\bar{k}_{\mathrm{r}} \\ 0 & \tilde{c} & (1+\chi\tilde{c})\tilde{u} \end{bmatrix}^{n+1,v},$$

$$\mathbf{C}^{(n+1,v)} = \begin{bmatrix} 0 & 0 & 0 \\ 0 & 0 & 0 \\ 0 & 0 & -C_w \dfrac{(1+\chi)}{(1+\chi\tilde{c})} \dfrac{2\tilde{c}}{\rho_{\mathrm{r}}} \end{bmatrix}^{n+1,v},$$

$$\mathbf{P}^{(n+1,v)} = \begin{bmatrix} 0 & 0 & 0 \\ 0 & \frac{4}{3}\mu_{\mathrm{t}}\dfrac{\partial}{\partial x}\left(\dfrac{1}{\bar{\rho}}\cdot\right) & \frac{4}{3}\mu_{\mathrm{t}}\dfrac{\partial}{\partial x}\left(\dfrac{\chi\tilde{u}}{\bar{\rho}}\cdot\right) \\ 0 & 0 & \dfrac{\mu_{\mathrm{t}}}{Sc_{\mathrm{t}}}\dfrac{\partial}{\partial x}\left(\dfrac{1+\chi\tilde{c}}{\bar{\rho}}\cdot\right) \end{bmatrix}^{n+1,v}, \qquad \mathbf{G}^{(n+1,v)} = \begin{bmatrix} 0 & 0 & -\beta\chi \\ 0 & 1 & 0 \\ 0 & 0 & 1 \end{bmatrix}^{n+1,v}. \tag{23}$$

In the above expression of **P**, the dot indicates that the spatial derivative has to be taken after the matrix product involving **P** in (13) has been performed.

4.1. Mesh and discretization

A classical staggered mesh $\mathscr{M}$ of nx points is used to spatially discretize the equations of (13). With the corresponding mesh stencil, displayed in Figure 2, the vector $\Delta\boldsymbol{q}^{\mathrm{ac}}$ is given by:

$$[\Delta \boldsymbol{q}^{\mathrm{ac}}]_i^{n+1,v} = \begin{bmatrix} [\Delta \bar{p}]_{i-1/2}^{n+1,v} \\ [\Delta \bar{\rho}\tilde{u}]_i^{n+1,v} \\ [\Delta \bar{\rho}\tilde{c}]_i^{n+1,v} \end{bmatrix} = \begin{bmatrix} [\Delta q_1^{\mathrm{ac}}]_{i-1/2}^{n+1,v} \\ [\Delta q_2^{\mathrm{ac}}]_i^{n+1,v} \\ [\Delta q_3^{\mathrm{ac}}]_i^{n+1,v} \end{bmatrix}, \tag{24}$$

with $i \in [2, nx-1]$.

The spatial derivatives $\partial/\partial x$ appearing in (13) and in the expression of $\mathbf{P}$ are calculated by considering a uniform computational mesh ξ via the relation:

$$\frac{\partial}{\partial x} = \frac{\partial \xi}{\partial x}\frac{\partial}{\partial \xi}. \tag{25}$$

The different Jacobians $\partial\xi/\partial x$ are deduced from the physical mesh and the form of the stencil given in Figure 2, namely:

$$\xi_{x_p}(i) = \frac{2\Delta\xi}{x_u(i) - x_u(i-1)},$$

for velocity and progress variable derivatives at pressure nodes.

$$\xi_{x_u}(i) = \frac{2\Delta\xi}{x_p(i+1) - x_p(i)}, \quad \text{for pressure derivatives at velocity nodes.}$$

$$\xi_x(i) = \frac{4\Delta\xi}{x_u(i+1) - x_u(i-1)},$$

for velocity and progress variable derivatives at velocity nodes. (26)

With $\Delta\xi = 1$, the different non-zero terms of (13) are discretized as follows:

Convective terms

$$\left[\frac{\partial}{\partial x} A_{12}.[\Delta q_2^{\mathrm{ac}}]\right]_{i-1/2}^{n+1,v} \simeq \xi_{x_p}(i)[A_{12}|_i^{n+1,v}\,[\Delta q_2^{\mathrm{ac}}]_i^{n+1,v} - A_{12}|_{i-1}^{n+1,v}\,[\Delta q_2^{\mathrm{ac}}]_{i-1}^{n+1,v}],$$

$$\left[\frac{\partial}{\partial x} A_{21}.[\Delta q_1^{\mathrm{ac}}]\right]_i^{n+1,v} \simeq \xi_{x_u}(i)[A_{21}|_{i+1/2}^{n+1,v}\,[\Delta q_1^{\mathrm{ac}}]_{i+1/2}^{n+1,v} - A_{21}|_{i-1/2}^{n+1,v}\,[\Delta q_1^{\mathrm{ac}}]_{i-1/2}^{n+1,v}],$$

$$\left[\frac{\partial}{\partial x} A_{lm}.[\Delta q_m^{\mathrm{ac}}]\right]_i^{n+1,v} \simeq \frac{\xi_x(i)}{2}[A_{lm}|_{i+1}^{n+1,v}\,[\Delta q_m^{\mathrm{ac}}]_{i+1}^{n+1,v} - A_{lm}|_{i-1}^{n+1,v}\,[\Delta q_m^{\mathrm{ac}}]_{i-1}^{n+1,v}],$$

with $(l, m) \in \{(2,2), (2,3), (3,2), (3,3)\}$.

Diffusion terms

$$\left[\frac{\partial}{\partial x} P_{22}.[\Delta q_2^{\mathrm{ac}}]\right]_i^{n+1,v} \simeq d_2^+ \frac{1}{\bar{\rho}}\Big|_{i+1}^{n+1,v} [\Delta q_2^{\mathrm{ac}}]_{i+1}^{n+1,v} + d_2 \frac{1}{\bar{\rho}}\Big|_i^{n+1,v} [\Delta q_2^{\mathrm{ac}}]_i^{n+1,v} + d_2^- \frac{1}{\bar{\rho}}\Big|_{i-1}^{n+1,v} [\Delta q_2^{\mathrm{ac}}]_{i-1}^{n+1,v},$$

$$\left[\frac{\partial}{\partial x} P_{23}.[\Delta q_3^{\mathrm{ac}}]\right]_i^{n+1,v} \simeq d_2^+ \frac{\chi\tilde{u}}{\bar{\rho}}\Big|_{i+1}^{n+1,v} [\Delta q_3^{\mathrm{ac}}]_{i+1}^{n+1,v} + d_2 \frac{\chi\tilde{u}}{\bar{\rho}}\Big|_i^{n+1,v} [\Delta q_3^{\mathrm{ac}}]_i^{n+1,v} + d_2^- \frac{\chi\tilde{u}}{\bar{\rho}}\Big|_{i-1}^{n+1,v} [\Delta q_3^{\mathrm{ac}}]_{i-1}^{n+1,v},$$

$$\left[\frac{\partial}{\partial x} P_{33}.[\Delta q_3^{\mathrm{ac}}]\right]_i^{n+1,v} \simeq d_3^+ \frac{1+\chi\tilde{c}}{\bar{\rho}}\Big|_{i+1}^{n+1,v} [\Delta q_3^{\mathrm{ac}}]_{i+1}^{n+1,v} + d_3 \frac{1+\chi\tilde{c}}{\bar{\rho}}\Big|_i^{n+1,v} [\Delta q_3^{\mathrm{ac}}]_i^{n+1,v} + d_3^- \frac{1+\chi\tilde{c}}{\bar{\rho}}\Big|_{i-1}^{n+1,v} [\Delta q_3^{\mathrm{ac}}]_{i-1}^{n+1,v},$$

with

$$d_2^+\big|_{i+1}^{n+1,v} = \xi_{x_u}(i)\xi_{x_p}(i+1)\left(\Theta \frac{4\mu_t}{3}\Big|_{i+1}^{n+1,v} + \Sigma \frac{4\mu_t}{3}\Big|_i^{n+1,v}\right),$$

$$d_3^+\big|_{i+1}^{n+1,v} = \xi_{x_u}(i)\xi_{x_p}(i+1)\left(\Theta \frac{\mu_t}{Sc_t}\Big|_{i+1}^{n+1,v} + \Sigma \frac{\mu_t}{Sc_t}\Big|_i^{n+1,v}\right),$$

$$d_2^-\big|_{i-1}^{n+1,v} = \xi_{x_u}(i)\xi_{x_p}(i)\left(\Omega \frac{4\mu_t}{3}\Big|_{i-1}^{n+1,v} + \Gamma \frac{4\mu_t}{3}\Big|_i^{n+1,v}\right),$$

$$d_3^-\big|_{i-1}^{n+1,v} = \xi_{x_u}(i)\xi_{x_p}(i)\left(\Omega \frac{\mu_t}{Sc_t}\Big|_{i-1}^{n+1,v} + \Gamma \frac{\mu_t}{Sc_t}\Big|_i^{n+1,v}\right),$$

$$d_2\big|_{i-1}^{n+1,v} = -(d_2^+\big|_{i+1}^{n+1,v} + d_2^-\big|_{i-1}^{n+1,v}); \qquad d_3\big|_{i-1}^{n+1,v} = -(d_3^+\big|_{i+1}^{n+1,v} + d_3^-\big|_{i-1}^{n+1,v})$$

and

$$\Theta = \left[\frac{x_p(i+1) - x_u(i)}{x_u(i+1) - x_u(i)}\right]; \qquad \Sigma = \left[\frac{x_u(i+1) - x_p(i+1)}{x_u(i+1) - x_u(i)}\right]; \qquad \Omega = \left[\frac{x_p(i) - x_u(i-1)}{x_u(i) - x_u(i-1)}\right];$$

$$\Gamma = \left[\frac{x_u(i) - x_p(i)}{x_u(i) - x_u(i-1)}\right].$$

Unsteady terms

$$[G_{13}.[\Delta q_3^{\mathrm{ac}}]]_{i-1/2}^{n+1,v} \simeq \Omega G_{13}\big|_i^{n+1,v} [\Delta q_3^{\mathrm{ac}}]_i^{n+1,v} + \Gamma G_{13}\big|_{i-1}^{n+1,v} [\Delta q_3^{\mathrm{ac}}]_{i-1}^{n+1,v}.$$

The final form of (13) is now written as:

$$\boldsymbol{\alpha}^{n+1,v}.[\Delta \boldsymbol{q}^{\mathrm{ac}}]_{i+1}^{n+1,v} + \boldsymbol{\delta}^{n+1,v}.[\Delta \boldsymbol{q}^{\mathrm{ac}}]_i^{n+1,v} + \boldsymbol{\gamma}^{n+1,v}.[\Delta \boldsymbol{q}^{\mathrm{ac}}]_{i-1}^{n+1,v} = \Delta\tau \mathrm{RHS}_i^{n+1,v}, \tag{27}$$

where matrices $\boldsymbol{\alpha}$, $\boldsymbol{\delta}$ and $\boldsymbol{\gamma}$ are given by:

$$\boldsymbol{\alpha}^{n+1,v} = \begin{bmatrix} 0 & 0 & 0 \\ \xi_{x_u}(i)\Delta\tau & \xi_x(i)\Delta\tau\tilde{u} - \Delta\tau d_2^+ \dfrac{1}{\bar{\rho}} & \xi_x(i)\Delta\tau\tilde{u}\left[\dfrac{\chi\tilde{u}^2}{2} - \dfrac{1}{3}\chi k_r\right] - \Delta\tau d_2^+ \dfrac{\chi\tilde{u}}{\bar{\rho}} \\ 0 & \xi_x(i)\Delta\tau\dfrac{\tilde{c}}{2} & \xi_x(i)\Delta\tau\left[\dfrac{(1+\chi\tilde{c})\tilde{u}}{2}\right] - \Delta\tau d_3^+ \dfrac{1+\chi\tilde{c}}{\bar{\rho}} \end{bmatrix}_{i+1}^{n+1,v}, \tag{28}$$

$$\boldsymbol{\delta}^{n+1,v} = \begin{bmatrix} 1 & \xi_{x_p}(i)\Delta\tau\beta & -\dfrac{3}{2}\dfrac{\Delta\tau}{\Delta t}\Omega\beta\chi \\ -\xi_{x_u}(i)\Delta\tau & 1 + \dfrac{3}{2}\dfrac{\Delta\tau}{\Delta t} - \Delta\tau d_2\dfrac{1}{\bar{\rho}} & -\Delta\tau d_2\dfrac{\chi\tilde{u}}{\bar{\rho}} \\ 0 & 0 & 1 + \dfrac{3}{2}\dfrac{\Delta\tau}{\Delta t} - \Delta\tau d_3\dfrac{1+\chi\tilde{c}}{\bar{\rho}} + C_w\dfrac{1+\chi}{(1+\chi\tilde{c})\rho_r}2\tilde{c} \end{bmatrix}_{i}^{n+1,v}, \tag{29}$$

$$\boldsymbol{\gamma}^{n+1,v} = \begin{bmatrix} 0 & -\xi_{x_p}(i)\Delta\tau\beta & -\dfrac{3}{2}\dfrac{\Delta\tau}{\Delta t}\Gamma\beta\chi \\ 0 & -\xi_x(i)\Delta\tau\tilde{u} + \Delta\tau d_2^-\dfrac{1}{\bar{\rho}} & -\xi_x(i)\Delta\tau\left[\dfrac{\chi\tilde{u}^2}{2} - \dfrac{1}{3}\chi k_r\right] + \Delta\tau d_2^-\dfrac{\chi\tilde{u}}{\bar{\rho}} \\ 0 & -\xi_x(i)\Delta\tau\dfrac{\tilde{c}}{2} & -\xi_x(i)\Delta\tau\left[\dfrac{(1+\chi\tilde{c})\tilde{u}}{2}\right] + \Delta\tau d_3^-\dfrac{1+\chi\tilde{c}}{\bar{\rho}} \end{bmatrix}_{i-1}^{n+1,v}, \tag{30}$$

$$\begin{aligned} \mathrm{RHS}_i^{n+1,v} = \Bigg[& -\xi_{x_p}(i)[\beta\bar{\rho}u|_i^{n+1,v} - \beta\bar{\rho}\tilde{u}|_{i-1}^{n+1,v}] - \Omega\left[3\frac{\beta\bar{\rho}|_i^{n+1,v} - \beta\bar{\rho}|_i^n}{2\Delta t} - \frac{\beta\bar{\rho}|_i^n - \beta\bar{\rho}|_i^{n-1}}{2\Delta t}\right] \\ & - \Gamma\left[3\frac{\beta\bar{\rho}|_{i-1}^{n+1,v} - \beta\bar{\rho}|_{i-1}^n}{2\Delta t} - \frac{\beta\bar{\rho}|_{i-1}^n - \beta\bar{\rho}|_{i-1}^{n-1}}{2\Delta t}\right] \\ & - \frac{\xi_x(i)}{2}\left[\left(\bar{\rho}\tilde{u}^2 - \frac{2}{3}\bar{\rho}k_r\right)\Big|_{i+1}^{n+1,v} - \left(\bar{\rho}\tilde{u}^2 - \frac{2}{3}\bar{\rho}k_r\right)\Big|_{i-1}^{n+1,v}\right] - \xi_{x_u}(i)[\bar{p}|_{i+1/2}^{n+1,v} - \bar{p}|_{i-1/2}^{n+1,v}] \\ & + \xi_{x_u}(i)\xi_{x_p}(i+1)(d_2^+\tilde{u}|_{i+1}^{n+1,v} - d_2\tilde{u}|_i^{n+1,v} + d_2^-\tilde{u}|_{i-1}^{n+1,v}) - 3\frac{\bar{\rho}\tilde{u}|_{i-1}^{n+1,v} - \bar{\rho}\tilde{u}|_{i-1}^n}{2\Delta t} \\ & + \frac{\bar{\rho}\tilde{u}|_{i-1}^n - \bar{\rho}\tilde{u}|_{i-1}^{n-1}}{2\Delta t} \\ & - \frac{\xi_x(i)}{2}[\bar{\rho}\tilde{u}\tilde{c}|_{i+1}^{n+1,v} - \bar{\rho}\tilde{u}\tilde{c}|_{i-1}^{n+1,v}] + \xi_{x_u}(i)\xi_{x_p}(i+1)(d_3^+\tilde{c}|_{i+1}^{n+1,v} - d_3\tilde{c}|_i^{n+1,v} + d_3^-\tilde{c}|_{i-1}^{n+1,v}) \\ & + C_w(1+\chi)\frac{(\tilde{c} - \chi c^*)(i-\tilde{c})}{(1+\chi\tilde{c})^2} - 3\frac{\bar{\rho}\tilde{c}|_{i-1}^{n+1,v} - \bar{\rho}\tilde{c}|_{i-1}^n}{2\Delta t} + \frac{\bar{\rho}\tilde{c}|_{i-1}^n - \bar{\rho}\tilde{c}|_{i-1}^{n-1}}{2\Delta t} \Bigg] \end{aligned}. \tag{31}$$

The block tridiagonal system (27) is then solved by a standard LU algorithm.

4.2. Adaptive gridding procedure

In order to minimize the number of grid points, while preserving a high level of spatial accuracy, an adaptive gridding procedure [20,21] is combined with the present time-accurate scheme. The staggered mesh $\mathscr{M}$ in the physical domain is chosen such that the two following constraints on the gradient and on the curvature of the $\tilde{c}$ profile are simultaneously satisfied everywhere in the domain:

$$\int_{x_i}^{x_{i+1}} \left|\frac{\partial \tilde{c}}{\partial x}\right| \mathrm{d}x \leq \epsilon_1 |\max \tilde{c} - \min \tilde{c}|, \quad i = 1, \ldots, nx-1 \tag{32}$$

and

$$\int_{x_i}^{x_{i+1}} \left|\frac{\partial^2 \tilde{c}}{\partial x^2}\right| \mathrm{d}x \leq \epsilon_2 \left|\max \frac{\partial \tilde{c}}{\partial x} - \min \frac{\partial \tilde{c}}{\partial x}\right|, \quad i = 1, \ldots, nx-1. \tag{33}$$

Thus grid points are concentrated in regions of high activity, thereby guaranteeing the accuracy of the numerical results. The values of the small numbers ϵ_1 and ϵ_2 are typically around 0.05.

4.3. Boundary and initial conditions

The choice of the boundary conditions to be imposed at the reactants side ($x = x_\mathrm{r}$) and at the burnt products side ($x = x_\mathrm{b}$) is dictated by the subsonic nature of the flow, which imposes the number of variables that should be specified or extrapolated.

At $x = x_\mathrm{r}$, the velocity $\overline{u_\mathrm{r}}$ and the progress variable are fixed. More precisely, the value of $\tilde{c}$ is chosen to be compatible with the asymptotic behavior of the solution given by Sabel'nikov *et al.* [18], namely:

$$\tilde{c}(x = x_\mathrm{r}) = \frac{\chi c^*}{(1 + \chi^2 c^*) \exp[+(mSc_\mathrm{t}/\rho_\mathrm{r}\mu_\mathrm{t})(x^* - x_\mathrm{r})] - \chi^2 c^*}, \tag{34}$$

where x^* represents the x-location of the point at which $\tilde{c} = \chi c^*$. At $x = x_\mathrm{b}$, the static pressure $p(x_\mathrm{b}) = p_\mathrm{b}$ is kept constant and serves as reference value for the pressure field, and the velocity and progress variables are extrapolated by assuming a zero curvature of their profiles. At time $t = 0$, the velocity and the pressure are set everywhere to $\overline{u_\mathrm{r}}$ and p_b respectively. The initial profile of $\tilde{c}$ is chosen to vary between x_r and x_b as follows:

$$\begin{cases} \forall x \in [x_\mathrm{r}, x_1] & \tilde{c} = \tilde{c}(x = x_\mathrm{r}), \\ \forall x \in [x_1, x_2] & \tilde{c} = \dfrac{x - x_1}{x_2 - x_1}, \\ \forall x \in [x_2, x_\mathrm{b}] & \tilde{c} = 1. \end{cases} \tag{35}$$

According to this choice, the mean flame brush will propagate towards the origin of the domain as schematically shown in Figure 1.

5. RESULTS

The resulting flow chart of the program is presented in Figure 3. At each physical time step, two nested loops of convergence are performed. The first loop corresponds to the convergence

of the iteration cycle in τ on a given mesh and the second corresponds to the convergence of the gridding procedure. Typically, three or four gridding steps are necessary per physical time step. Two different types of propagating flames are considered, a slow flame ($\chi = 5$, $S_{t_0} = 0.5$ m s^{-1}, test case 1) and a fast flame ($\chi = 5$, $S_{t_0} = 10$ m s^{-1}, test case 2). When not stated otherwise, the values of all the different parameters that describe the present calculations are given in Table I.

Figure 4 presents, for case 2, a typical evolution of the maxima of the residuals of the RHS (Equation (31)) during the course of the iteration cycle in τ combined with the gridding procedure. On a given mesh, these residuals are experiencing a quasi-monotonic decrease. Practically, the iteration cycle in τ is considered to be converged when the maxima of all the residuals are below 10^{-5}, since no noticeable changes in the profiles have been observed when a more stringent criterion is adopted. An illustration of the propagation of the mean flame

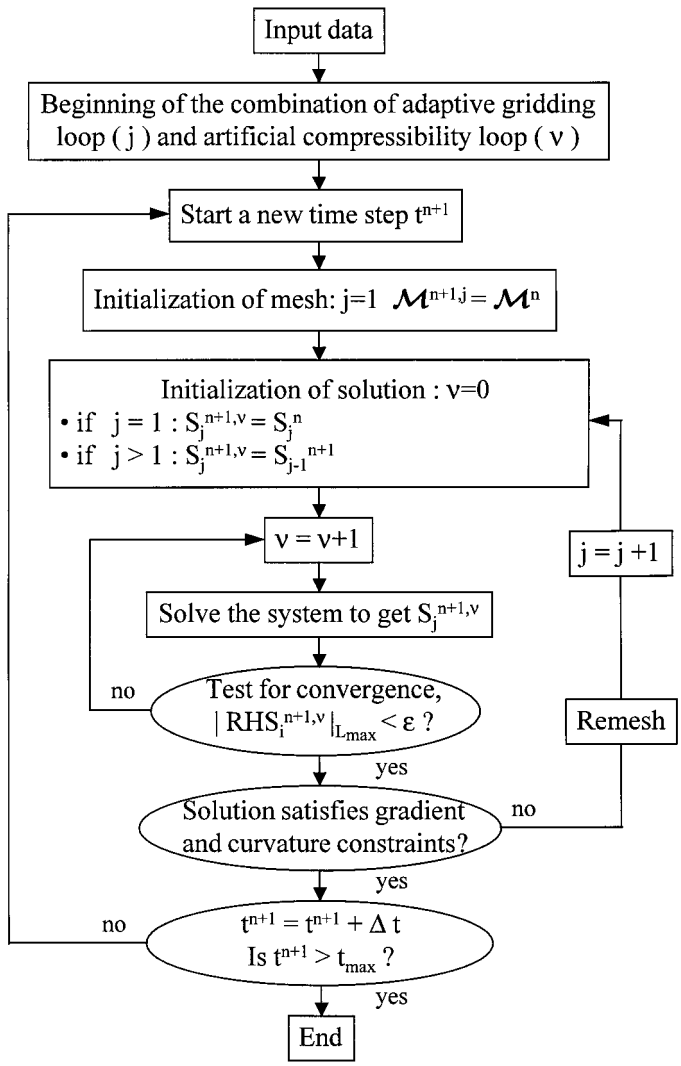

Figure 3. Flow chart of the program.

Table I. Parameters defining the two test cases

Case	1	2
χ	5.0	5.0
u_r (m s^{-1})	0.0	0.0
u'_r (m s^{-1})	1.0	10.0
χc^*	0.03958	0.03958
S_{t_0} (m s^{-1})	0.5	10.0
l_i (m)	0.001	0.001
Sc_t	0.75	0.75
C_w (kg m^{-3} s^{-1})	200	8000
ρ_r (kg m^{-3})	1.1886	1.1886
x_r (m)	0.0	0.0
x_b (m)	0.50	0.20
x_1 (m)	0.40	0.10
x_2 (m)	0.45	0.15
β	10.0	10.0
Cr_τ	1000	1000
Cr_t	0.50	0.50

brush is presented in Figure 5, which displays the time evolution of the profile $\tilde{c}(x)$ for case 1. At 20 ms, the steady regime of propagation is reached and the mean flame brush structure becomes invariant by translation. This fact is clearly illustrated in Figure 6, which presents, for

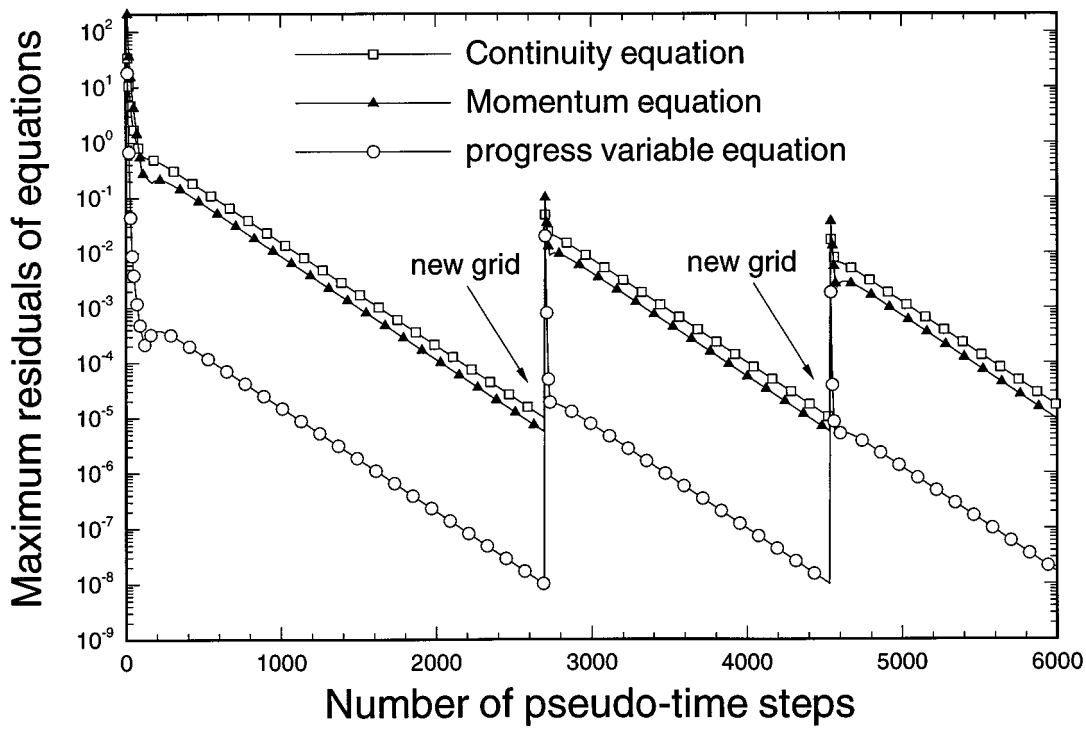

Figure 4. Example of the convergence history of the two nested loops of artificial compressibility iteration and remeshing for one physical time step (case 2, $Cr_t = 0.5$, $Cr_\tau = 1000$).

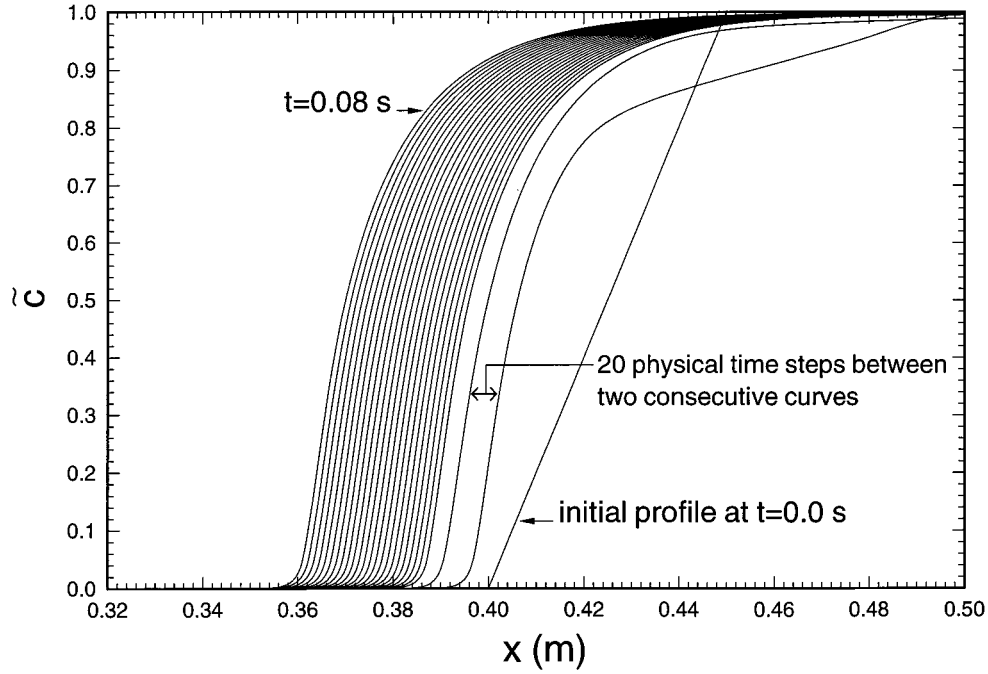

Figure 5. Calculated propagation of the mean flame brush (case 1, $Cr_t = 0.5$, $Cr_\tau = 1000$).

case 1, the time evolution of the x-location at which $\tilde{c} = 0.1$, 0.5 and 0.9. The trajectories of these three points are becoming straight and parallel as soon as $t > 20$ ms, indicating that from this instant onwards, the corresponding points travel at the same constant speed, which is a signature of the invariance by translation of the mean flame brush structure. The reactants being at rest in average ($\overline{u_r} = 0$), the mean flame brush velocity relative to the reactants, S_t, is simply given by the slope of one of these trajectories, for instance $S_t = |\mathrm{d}x_{\tilde{c}=0.5}/\mathrm{d}t|$. As illustrated in Figure 7, in both cases, the value of S_t predicted by the present time-accurate scheme asymptotically approaches the value S_{t_0} that corresponds to the quenching value χc^*. Correctly predicting the mean flame brush asymptotic propagation velocity is encouraging as far as the time accuracy of the scheme is concerned, but how accurately calculated is the mean flame brush structure? To answer this question, the calculated limit profiles, i.e. the profiles obtained when a steady regime of propagation is reached, are compared with those obtained using the Runge–Kutta procedure developed by Sabel'nikov *et al.* [18] in the framework of a KPP approach. Whether it is for the $\tilde{c}$ profile (Figure 8) or for the mean pressure gradient profile (Figure 9), the agreement between the present results and those given by the KPP approach is excellent, even in the case of the fastest flame (case 2), for which the present scheme proves its ability to accurately capture the steep pressure gradient that exists through the mean flame brush. These results clearly illustrate the capability of the present scheme to deal with unsteady reacting flows featuring large density variations. The problem now faced by the potential end-user of the present time-accurate scheme is the following: what is the best choice for β and $\Delta\tau$? Although the answer to this question is highly dependent on the geometry considered and the time scale associated with the unsteadiness of the flow, some guidelines can be deduced in the present flow geometry from a sensitivity analysis of the convergence rate of the calculations to the choice of these parameters. The influence of the

artificial compressibility factor β can be investigated by reference to a reduced artificial compressibility factor $\tilde{\beta} = \beta / u_{\mathrm{ref}}^2$, where the reference velocity depends on the flow considered [22]. For reacting flows, a proper scaling of β is given by $u_{\mathrm{ref}} = \overline{u_{\mathrm{b}}}$, where $\overline{u_{\mathrm{b}}}$ is the characteristic velocity of the burnt products [5]. For the present flow geometry, $\overline{u_{\mathrm{b}}}$ is estimated by $\overline{u_{\mathrm{b}}} = \overline{u_{\mathrm{r}}} + \chi S_{t_0}$, which represents the velocity of the burnt products behind the mean flame brush. The sensitivity of the convergence rate to the value of $\Delta\tau$ is performed by analyzing the influence of an artificial Courant number based on the largest spectral radius obtained in the domain of calculation and associated with the inviscid part of the equations, namely [5,22]:

$$Cr_\tau = \frac{\Delta\tau}{\Delta x}\left(\overline{u_{\mathrm{b}}} + \sqrt{\overline{u_{\mathrm{b}}}^2 + \beta}\right). \tag{36}$$

The influence of the physical time step Δt is strongly connected to the method of resolution. In particular, for multidimensional flows, it is well-known for instance, that the use of an approximate factorization scheme imposes a limitation on the value of $(\beta \Delta t)$, whereas the recourse to a relaxation procedure does not. For the present 1D geometry, a physical Courant number Cr_t that takes into account the time scale associated with the flame brush propagation is chosen. Accordingly, Cr_t is defined by:

$$Cr_t = \frac{\Delta t}{\Delta x} S_{t_0}. \tag{37}$$

The use of an adaptive gridding procedure complicates the choice of Δx in the above expressions of Cr_τ and Cr_t, since the non-uniform mesh changes during the course of the calculations. Thus, Cr_τ and Cr_t are calculated by using the smallest value of Δx of the current

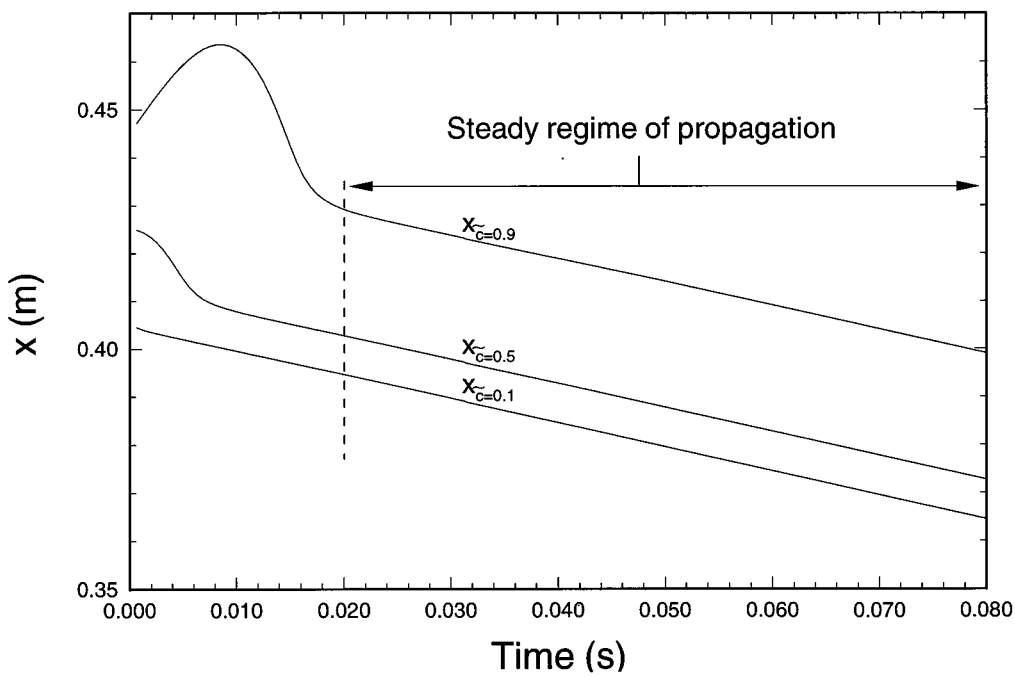

Figure 6. Time evolution of the spatial location of points $\tilde{c} = 0.1$, $\tilde{c} = 0.5$ and $\tilde{c} = 0.9$ that belong to the propagating mean flame brush (case 1, $Cr_t = 0.5$, $Cr_\tau = 1000$).

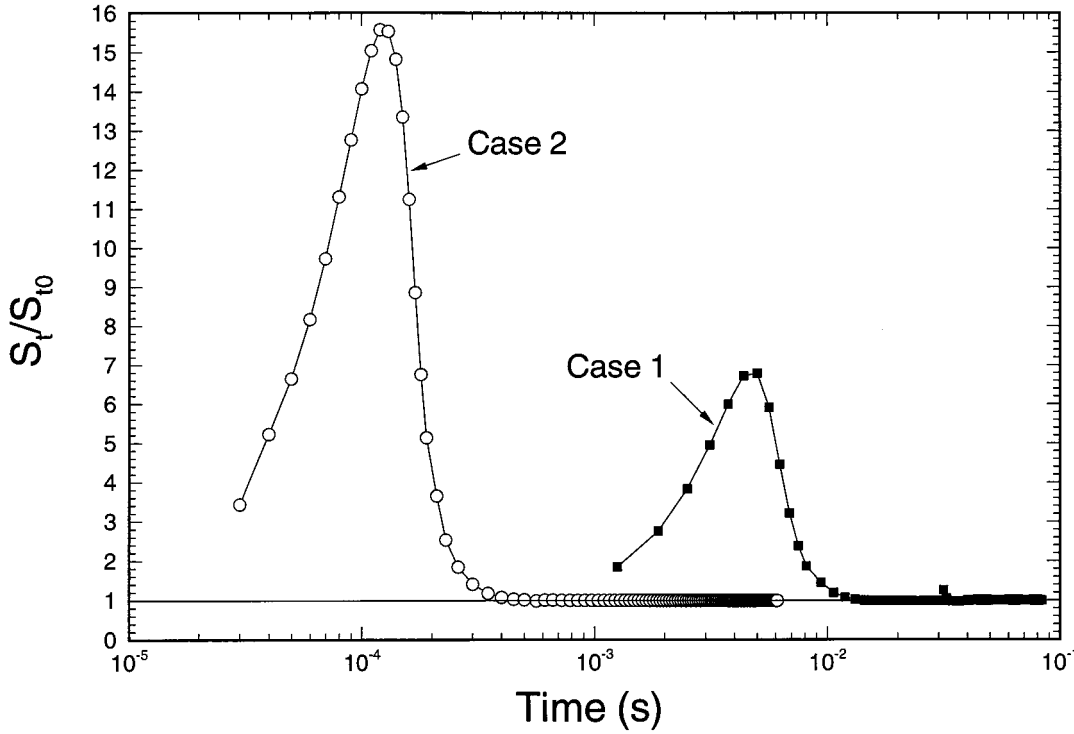

Figure 7. Time evolution of the mean flame brush propagation velocity ($Cr_t = 0.5$, $Cr_\tau = 1000$).

mesh. The sensitivity analysis is performed in case 2, when the mean flame brush has reached its steady regime of propagation at a velocity of 10 m s^{-1}. In such a regime, the value of Δx used to calculate Cr_τ and Cr_t remains quasi-constant as does $\Delta\tau$ and Δt as soon as Cr_τ and Cr_t are kept constant. The number of accumulated pseudo-time steps needed to calculate the flame displacement during a period of time of 0.15 ms is chosen to reveal the influence of the parameters values on the convergence rate. Figure 10 shows that, for a reasonable value of $Cr_t = 0.5$ (corresponding to $\Delta t = 1.25 \times 10^{-5}$ s), a value of $\hat{\beta}$ between 5 and 10 optimizes the rate of convergence. Such a result is similar to that obtained for the calculations of steady inert or reacting flows. For such an optimum value of $\hat{\beta}$, the value of Cr_τ found to optimize the convergence rate of the present unsteady calculations is in the range 1000–1400, which is much larger than the value of 45 found in the steady calculations [5]. Such a difference is easily explained if one considers that for the present unsteady calculations, the solution obtained at the previous time step represents a much better initial guess to the solution at the next time step; whereas for steady calculations, the initial guess can be extremely different from the converged solution, thus imposing a much smaller value of the artificial Courant number. As shown by Figure 11, increasing Cr_t from 0.5 to 1.5 leads to a slight shift of the range of optimal value of Cr_τ from 1000–1400 to 800–1200. It should be noted that, as soon as an optimal value of $\hat{\beta}$ is used, the sensitivity of the convergence rate to the value of Cr_τ is weak. For instance, for $\hat{\beta} = 5$ and $Cr_t = 1.5$, a variation of less than 20% of the number of accumulated pseudo-time steps is observed when Cr_τ varies between 500 and 1600.

From these results, the following recommendations can be made for roughly estimating the values of the parameters required by the present scheme:

1. determine a characteristic time scale associated with the unsteadiness of the reacting flow considered;
2. choose the physical time step Δt in order to obtain a moderate value (relative to the type of time integration used) of the physical Courant number based on this characteristic time scale;
3. determine the reference velocity u_{ref} as being the maximum convective velocity in the flow that will be, most of the time, found to be in the region of the burnt products;
4. set the value of β between $5u_{\text{ref}}^2$ and $10u_{\text{ref}}^2$;
5. for a given mesh, choose $\Delta\tau$ such that $Cr_\tau \simeq 500-1500$.

It is clear that the above practical and rather simple recommendations provide only a starting point for the potential end-user of the present time-accurate scheme especially when the calculations of multidimensional flows are to be considered.

6. CONCLUDING REMARKS

This work shows how the artificial compressibility approach can be used to derive a method of solution of unsteady reacting flow fields in the limit of a low Mach number. The resulting time-accurate scheme has been validated in two cases of 1D propagating turbulent flames with large density variations. Whether it is for the spatial accuracy of the calculated flame brush profiles or for the prediction of the flame brush propagation velocities, the present results are in excellent agreement with those obtained by an analysis of the steady regime of propagation. With the present extension, the last domain of applicability of the artificial compressibility

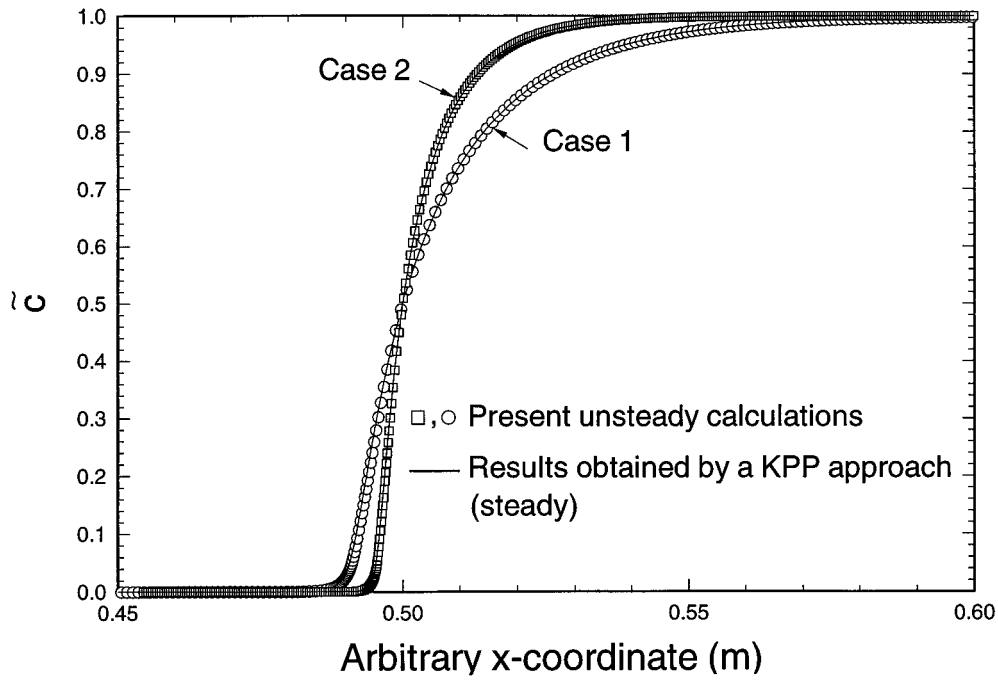

Figure 8. Limit profile of the mean progress variable obtained when a steady regime of propagation is achieved: comparison with the profile deduced from a steady regime analysis [18].

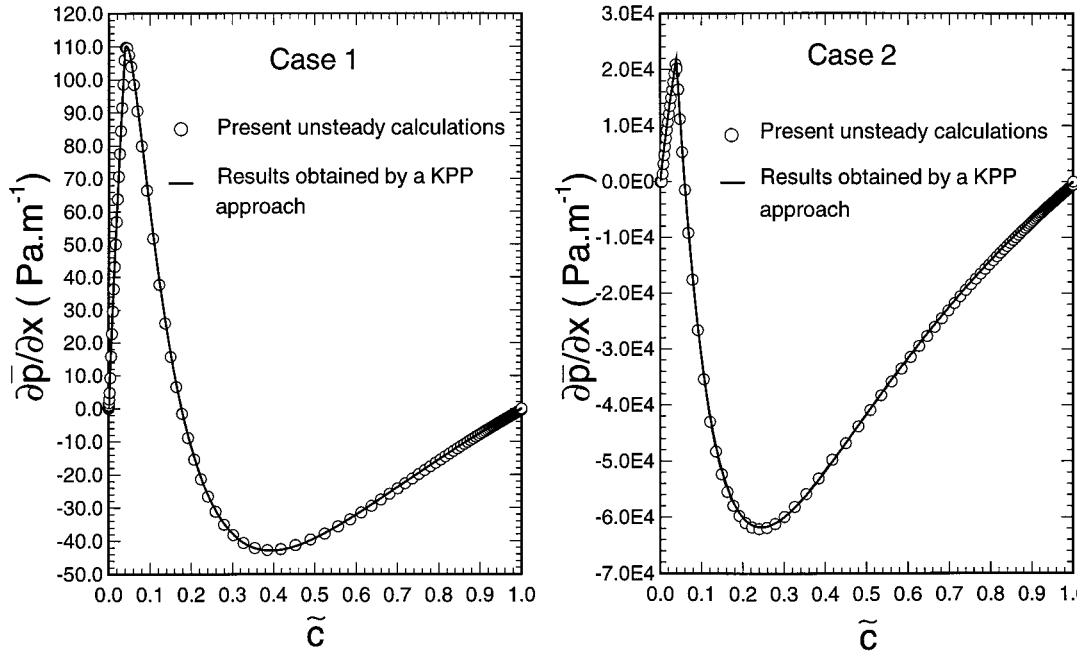

Figure 9. Limit profile of the mean pressure gradient obtained when a steady regime of propagation is achieved: comparison with the profile deduced from a steady regime analysis [18].

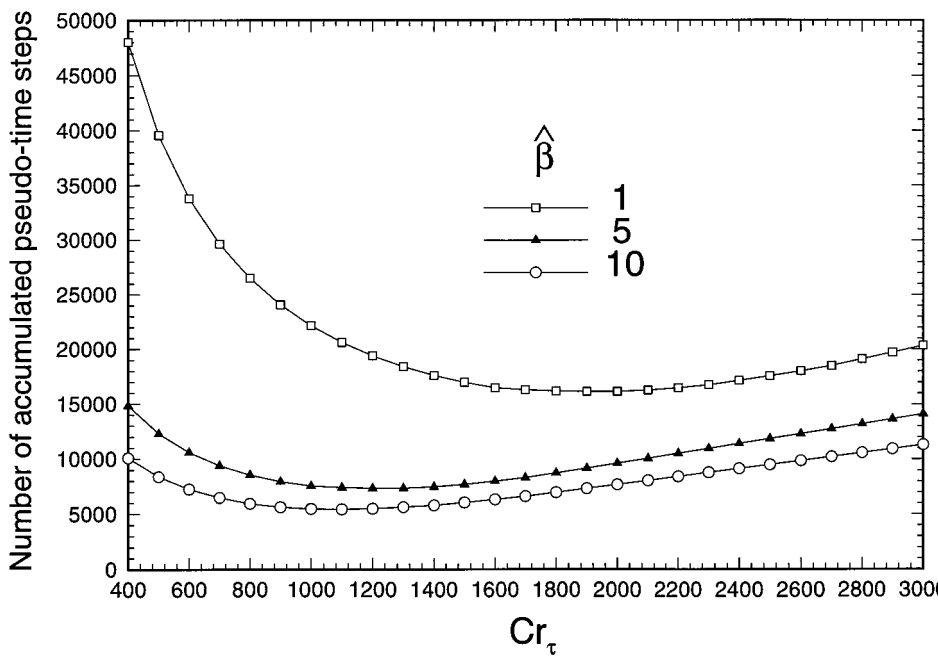

Figure 10. Influence of the artificial Courant number Cr_τ and the dimensionless artificial compressibility factor $\hat{\beta}$ on the convergence rate (case 2, $Cr_t = 0.5$, 12 physical time steps).

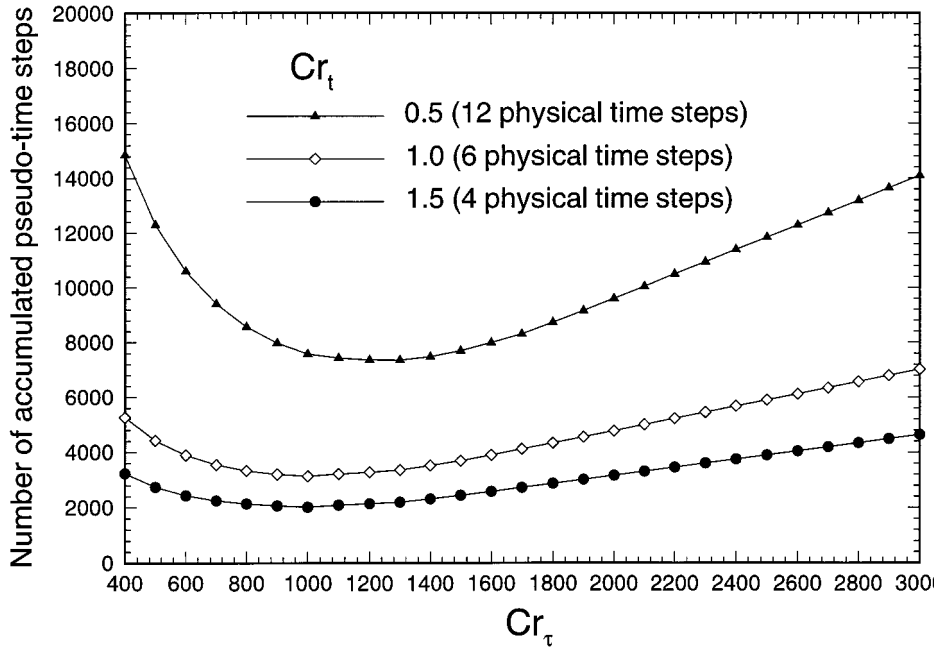

Figure 11. Influence of the Courant numbers Cr_τ and Cr_t on the convergence rate (case 2, $\hat{\beta} = 5.0$).

approach has been now explored. The extension of this scheme to multidimensional geometries can be easily considered, especially when using implicit-factored schemes for which the present scheme corresponds to one of the two (2D) or three (3D) fractional steps involved by such procedures. Thus, and as pointed out by in [12], the artificial compressibility method may not be the most efficient method for each class of flow it can deal with, but its now proven versatility and also the availability of specific techniques that can be used to greatly improve its efficiency for a given class of flows [10,13], make it a very attractive and valuable tool for CFD.

ACKNOWLEDGMENTS

Part of this work has been performed during a 3-month stay of Professor V.A. Sabel'nikov at the Laboratoire de Combustion et de Détonique as an Associate Researcher of the Centre National de la Recherche Scientifique.

REFERENCES

1. J.D. Buckmaster and G.S.S. Ludford, *Theory of Laminar Flames*, Cambridge University Press, Cambridge, 1982.
2. R.I. Issa, B. Ahmadi-Befrui, K.R. Beshay and A.D. Gosman, 'Solution of the implicitly discretised reacting flow equations by operator-splitting', *J. Comput. Phys.*, **93**, 388–410 (1991).
3. L.S. Caretto, A.D. Gosman, S.V. Patankar and D. B. Spalding, *Proc. 3rd Int. Conf. on Numerical Methods in Fluid Dynamics*, 1972.
4. A.J. Chorin, 'A numerical method for solving incompressible viscous flow problems', *J. Comput. Phys.*, **2**, 12–26 (1967).
5. P. Bruel, D. Karmed and M. Champion, 'A pseudo-compressibility method for reactive flows at zero Mach number', *Int. J. Comput. Fluid Dyn.*, **7**, 291–310 (1996).
6. D. Karmed, H. Lahjaily, P. Bruel and M. Champion, 'Influence of the turbulent Damkohler number on the structure of premixed flames in a stagnation flow', *Combust. Sci. Technol.*, **113–114**, 351–365 (1996).

7. R. Peyret, 'Unsteady evolution of a horizontal jet in a stratified fluid', *J. Fluid Mech.*, **78**, 49–63 (1976).
8. D. Choi and C.L. Merkle, 'Application of time-iterative schemes to incompressible flow', *AIAA J.*, **23**, 1518–1524 (1985).
9. W.Y. Soh and J.W. Goodrich, 'Unsteady solution of incompressible Navier–Stokes equations', *J. Comput. Phys.*, **79**, 113–134 (1988).
10. B. Granier, A. Lerat and Z.-N. Wu, 'An implicit centered scheme for steady and unsteady incompressible one- and two-phase flows', *Comput. Fluids*, **26**, 373–393 (1997).
11. S.E. Rogers and D. Kwak, 'Upwind differencing scheme for the time-accurate incompressible Navier–Stokes equations', *AIAA J.*, **28**, 253–262 (1990).
12. P.R. McHugh and J.D. Ramshaw, 'Damped artificial compressibility iteration scheme for implicit calculations of unsteady incompressible flow', *Int. J. Numer. Methods Fluids*, **21**, 141–153 (1995).
13. Th. Pappou and S. Tsangaris, 'Development of an artificial compressibility methodology using flux vector splitting', *Int. J. Numer. Methods Fluids*, **25**, 523–545 (1997).
14. D.B. Spalding, 'Mixing and chemical reaction in steady confined turbulent flames', *Proc. 13th Symp. (Int.) on Combustion*, The Combustion Institute, Pittsburgh, PA, 1971, pp. 649–657.
15. Y.B. Zel'dovich, G.I. Barenblatt, V.B. Librovich and G.M. Makhviladze, *The Mathematical Theory of Combustion and Explosions*. Plenum, New York, 1980.
16. K.N.C. Bray and P.A. Libby, 'Interaction effects in turbulent premixed flames', *Phys. Fluids*, **19**, 1687–1701 (1976).
17. C.A. Catlin and R.P. Lindstedt, 'Premixed turbulent burning velocities derived from mixing controlled reaction models with cold front quenching', *Combust. Flame*, **85**, 427–439 (1991).
18. V.A. Sabel'nikov, C. Corvellec and P. Bruel, 'Analysis of the influence of cold front quenching on the turbulent burning velocity associated with an eddy break-up model', *Combust. Flame*, **113**, 492–497 (1998).
19. P. Bruel, 'Numerical study of a one-dimensional turbulent flame', *Proc. 3rd Asian–Pacific Int. Symp. on Combustion and Energy Utilization*, Hong Kong, 1995, pp. 472–477.
20. V. Giovangigli and M.D. Smooke, 'Extinction of strained premixed laminar flames with complex chemistry', *Combust. Sci. Technol.*, **53**, 23–49 (1987).
21. P. Bruel, B. Rogg and K.N.C. Bray, 'On auto-ignition in laminar and turbulent non-premixed systems', *Proc. 23rd Symp. (Int.) on Combustion*, The Combustion Institute, Pittsburgh, PA, 1990, pp. 759–766.
22. W.Y. Soh, 'Time-marching solution of incompressible Navier–Stokes equations for internal flow', *J. Comput. Phys.*, **70**, 232–252 (1987).
23. R.M. Beam and R.F. Warming, 'An implicit factored scheme for the compressible Navier–Stokes equations', *AIAA J.*, **16**, 393–402 (1978).
24. A. Kolmogorov, I. Petrovskii and N. Piskunov, 'Study of the diffusion equation with growth of the quantity of matter and its application to a biology problem', *Bull. MGU, Moscow State University, A*, **1** (1937).

